ACS APPLIED ENERGY MATERIALS

Article

Cite This: ACS Appl. Energy Mater. 2020, 3, 868–878

www.acsaem.org

Radiation-Induced Evolution of Tungsten Carbide in Fusion Reactors: Accommodation of Defect Clusters and Transmutation Elements

Samuel X. Oliver,[†] Matthew L. Jackson,[‡] and Patrick A. Burr*[,§]

[†]Graduate School of Biomedical Engineering, University of New South Wales, Sydney, New South Wales 2052, Australia

[‡]Institute for Materials Discovery, University College London, London WC1E 7JE, United Kingdom

[§]School of Mechanical and Manufacturing Engineering, University of New South Wales, Sydney, New South Wales 2052, Australia

Supporting Information

ABSTRACT: The development of suitable shielding material is a key challenge in the advancement of spherical tokamak fusion reactors. Tungsten carbide (WC) is a promising candidate material owing to its low neutron and gamma attenuation lengths resulting from the combination of high-Z and low-Z elements, but its behavior under prolonged exposure to fusion neutrons is poorly understood. Here, we shed light on the microstructural evolution of WC under neutron irradiation by investigating the formation and clustering of defects using density functional theory atomic simulations. It is found that deviation from stoichiometry is accommodated entirely by C defects (vacancies and interstitials), while the disorder induced by radiation damage may be accommodated by three competing processes (C- Frenkel, antisite, and Schottky) with similar energetics. Vacancy clusters involving a combination of both tungsten and carbon vacancies show increasingly favorable binding energies with increasing cluster size and may lead to the formation of undesirable extended defects such as dislocation loops and voids. The accommodation of the three main transmutation elements Re, Os, and Ta was also considered, as well as their interaction with radiation-induced intrinsic defects. It was found that all three species are preferentially accommodated as substitution defects on the W sublattice, and they all exhibit a thermodynamic drive to bind with W vacancies, while Ta also binds with C vacancies and with Re and Os substitutions. This suggests that radiation-induced vacancy sinks (e.g., voids and dislocation loops) will likely be enriched in transmutation elements, and that these further stabilize the vacancy clusters, potentially aggravating swelling. However, it is predicted that under equilibrium conditions, all three species exhibit limited solubility in WC, assuming that the competing phases for precipitation are $TaC_{(s)}$, $Os_{(s)}$, and $Re_{(s)}$. Further investigation into the C-(Ta,Re,Os)-W phase diagram is needed to improve the accuracy of these predictions.

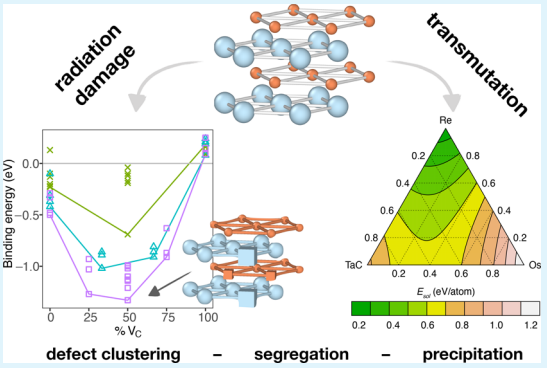

KEYWORDS: *tungsten carbide, defect chemistry, nuclear fusion, shielding, transmutation, defect clusters, radiation damage*

1. INTRODUCTION

Fusion tokamak reactors are a promising source of a sustainable and low-carbon energy, and their development is chiefly limited by advancements in material science. Spherical tokamaks are particularly promising owing to their compact size and associated reduced cost of development.[1] Here, the greatest technological challenge lies in the design of suitable materials capable of shielding the superconducting magnets from the radiation field generated within the reactor.[1,2]

Tokamak reactors rely on superconducting magnets to provide magnetic confinement of the fusion plasma. The complex metal oxide materials, such as $YBaCuO_3$, used for the magnetic coils are known to be strongly susceptible to radiation damage at the low temperatures required for the superconductive behavior (<93 K).[3] To enable sustained operation of a tokamak reactor, it is therefore crucial to shield these materials from neutron and γ radiation emitted from the plasma.

Radiation shielding is particularly challenging for the central column of spherical tokamaks, where space is at a premium.[2] For this tokamak design, replacing conventional shielding materials with more effective ones maximizes the space available for the magnetic coil and plasma, and therefore increases tokamak power density.

The ideal shielding material must primarily attenuate energetic neutrons from the D-T reaction, but also absorb gamma and X-rays produced through the interaction of these neutrons with the shielding material. Therefore, it must (a) have a reasonable macroscopic cross-section for neutron

Received: October 8, 2019
Accepted: December 6, 2019
Published: December 6, 2019

DOI: 10.1021/acsaem.9b01990
ACS Appl. Energy Mater. 2020, 3, 868–878

absorption (Σ_a), (b) be an effective neutron moderator (high macroscopic slowing down power, MSDP) and (c) have a large attenuation coefficient for high energy gamma (μ). This poses a material selection challenge since elements that exhibit high μ also have low MSDP, and vice versa. More precisely, the MSDP can be approximated to vary with the inverse of the atomic number $\left(\text{MSDP} \approx \Sigma_s \frac{2}{A+\frac{2}{3}}\right)$, while μ increases roughly linearly with atomic mass ($\mu \propto Z$).

Tungsten carbide exhibits a combination of high atomic packing, reasonably large thermal absorption cross-section of W ($\Sigma_a^{25\ \text{meV}}$ = 18.3 b, without isotopic enrichment[4]), large MSDP from C atoms, and large μ contribution from W. This favorable combination of nuclear properties, in addition to its excellent and extensively characterized thermophysical and manufacturing properties, make WC a promising candidate material for the shielding of components in spherical tokamak reactors,[5−8] as well as for the diverter in conventional tokamak reactors.[9−12]

The implicit consequence of exposing a material with non-negligible Σ_a (such as W) to a neutron field, is that the material will be transmuted to heavier isotopes, potentially changing the composition through decay of the newly generated isotopes. Gilbert and Sublet[13] have shown that exposing W to neutron fluxes typical of fusion tokamaks leads to the formation of considerable amounts of Ta, Re, and Os, reaching parts-per-thousand in under 1 year. Gilbert and Sublet[13] have also shown that all other activation products (Ir, Pt, Hf, H, He) only reach negligible concentrations even after 5 years of exposure. Similar concentrations are expected to form in WC; in fact, the presence of C, a strongly moderating element, may accelerate the formation of activation products. The presence of these transmutation elements may affect the physical and mechanical properties of the material, especially if they segregate into secondary phases or grain boundaries.

Tungsten carbide is a well-studied material, extensively used in cutting tools and high-wear components[14,15] owing to its extreme hardness (20.4 GPa),[16,17] high melting point (>3000 K) and excellent thermal stability and oxidation properties.[5,18] Owing to the layered hexagonal structure of WC, the material is expected to exhibit many anisotropic properties, including thermal conductivity[19] and chemical diffusivity.[20] This may also result in anisotropic swelling and grain boundary cracking, as has been observed in other layered hexagonal structures,[21−23] therefore directional swelling should be considered in component design via texture engineering.

Despite the importance of the material, few experimental studies have considered its use in radiation environments,[5−11] and even fewer irradiation experiments have been performed, chiefly in the 1970s with the aim of hardening the material for cutting tools.[24−27] This is in contrast to W metal, in which the microstructural evolution under irradiation, and the corresponding changes in material properties, have been extensively characterized through experimental irradiation with He,[28−33] H isotopes,[33−37] heavy ions,[28,38−43] and neutrons.[44−52] A particular concern of W (both alloyed and unalloyed), is the segregation of Re and Os transmutation products, first in the form of clusters within the W matrix and later as Re−Os-rich precipitates,[45,47,48] which are known to aggravate the radiation-induced embrittlement of W metal.[46,47] The fluence at which these precipitates appear, and when they start to dominate the degradation of the mechanical properties, is dependent on alloy type, temperature, and neutron flux.[50,52]

On the other hand, WC has been the subject of many atomic-scale computational studies, including investigation of bulk properties,[53] point defects,[20,54,55] self-diffusivity,[20] radiation damage,[56,57] and gas retention.[56,58−60] Previous DFT work[20,54,55] has shown that in dilute conditions, C vacancies are the most easily accommodated intrinsic point defects, followed by C interstitials (trigonal site on the C sublattice) and W vacancies, while W interstitials are highly unfavorable. This is evident from the formation energies of the respective defects, reproduced in Table 1. However, no DFT study thus far has considered the evolution of these point defects with increasing concentration due to the continued exposure to fusion neutrons. Additionally, no study has investigated whether transmutation products of W can be accommodated in WC.

Table 1. Formation Energy of Dilute Point Defects in WC[a]

defect	E_f (eV)
V_C	2.56
V_W	6.78
C_W	11.03
W_C	11.27
$C_{i\ (\text{TriC})}$	4.52
$W_{i\ (\text{TriC})}$	14.31

[a]For details of the naming convention, and comparison with other literature values, see ref 20. Only the lowest energy interstitial site for C and W is reported here, but other (less favorable) stable sites have also been reported.[20,54].

Here, we build on previous work by investigating the driving force for formation of defect clusters (section 3), which underpins the microstructural evolution of the material under irradiation, such as the nucleation of voids, interstitial loops, vacancy loops, and bubbles. We then re-examine the disorder processes in the material (section 4) by extending the analysis of previous work to include defect clusters as well as dilute defects, which appears to have a significant effect on the predicted disorder behavior of WC. In section 5, we consider the solubility of W transmutation products, and how these affect the radiation tolerance of the material. This is investigated both for dilute conditions and at higher concentrations by including the contribution of defect clusters. Finally, in section 6 the findings are summarized and conclusions regarding the suitability of WC as shielding material are drawn.

2. METHODOLOGY

2.1. Computational Details. All DFT simulations were carried out using the Vienna Ab-Initio Simulation Package (VASP)[61,62] using the PBE formalism of the generalized gradient approximation for exchange-correlation functional[63] and the D3 Van-der-Waals correction term of Grimme.[64] The post-DFT Van-der-Waals treatment has been shown to be important for the simulation of point defects in WC, and for an accurate description of graphite.[20,65,66]

Atoms were described with PAW pseudopotentials[67] from the VASP 5.3 repository with 4 and 14 valence electrons for C and W, respectively. A consistent plane-wave cutoff of 500 eV was used throughout. Ta, Re, and Os atoms were described with valence p electrons. As WC exhibits no band gap,[53] the

DOI: 10.1021/acsaem.9b01990
ACS Appl. Energy Mater. 2020, 3, 868−878

defects were calculated in charge neutral cells and the partial occupancies of bands were treated with a first-order Methfessel-Paxton smearing function of width 0.1 eV.[68]

The calculated lattice parameters, elastic constants, formation energies, and cohesive energies are in good agreement with previous DFT[53,58] and experimental work[16] (full details in the Supporting Information).

Defect calculations were performed in a prerelaxed 128 atom supercell, formed by 4 × 4 × 4 replicas of the conventional unit cell. This supercell is large enough to accommodate divacancy and trivacancy clusters with self-interaction energy less than 0.06 eV, as calculated through linear elastic theory using the *aneto* tool.[69] On the other hand, single W interstitials yielded non-negligible self-interaction energies of up to 0.65 eV. However, this finite size error remains below 5% of the defect formation energy, which is unusually large at 14 eV, and because of the large positive formation energy, these defects are not relevant under equilibrium conditions. Defect calculations were performed at constant volume (only internal degrees of freedom were minimized) from the relaxed supercells and without enforcing any symmetry operations. The convergence criteria for electronic and ionic minimization was 10^{-6} eV and 10^{-5} eV, respectively. K-point sampling of the Brillouin zone was performed with Γ-centered 3 × 3 × 3 Monkhorst−Pack grids[70] for the supercell.

2.2. Formation Energy and Binding Energy Definition. The formation energy (E_f) is defined according to

$$E_f = E^{DFT}(\text{defect}) - E^{DFT}(\text{perfect}) \pm n\mu_x \quad (1)$$

where E^{DFT}(defect) and E^{DFT}(perfect) are the DFT total energies of the defective and perfect supercells (of same size), and μ_x is the energy of any atoms (n) that is added or removed from the perfect crystal to create the defect. This was taken from a DFT calculation of the ground state structure of the elemental material: graphite, bcc-W, bcc-Ta, hcp-Re, and hcp-Os. For extrinsic species, we also considered the equivalent defect formation reaction where the chemical reservoir of extrinsic species are their monocarbides (TaC, ReC, OsC), as these are phases that may potentially form over the elemental metals in a C-rich environment.

Note that eq 1, applied to extrinsic defects, also defines the solution energy of the extrinsic species X in WC. For instance, in the case a of a substitution onto the W sublattice, the solution reaction is

$$X_{(s)} + W_W \rightarrow X_W + W_{(s)}$$

However, it is important to note that Ta, Re, and Os are formed by the transmutation of W, and therefore, unlike conventional defect chemistry, the reactions are necessarily not mass balanced. Specifically, when considering a transmutation of W, the W atom is not displaced by the transmutation element, but it is instead *replaced* by it. In this scenario, more relevant reactions maybe

$$W_W \xrightarrow{(n,\beta^+)} Ta_W \Rightarrow Ta_W + WC_{(s)} \rightarrow TaC_{(s)} + W_W$$

or

$$W_W \xrightarrow{(n,\beta^-)} Re_W \Rightarrow Re_W \rightarrow Re_{(s)} + V_W$$

But these are only two of many potential (competing) reactions. To ascertain which reaction would dictate the partitioning of Ta, Re, and Os in a neutron-irradiated WC requires greater knowledge of the thermodynamic stability of ternary, quaternary, and quinary phases in the C−(Ta,Re,Os)−W phase diagram, as well as precise knowledge of the W/C stoichiometry. As there are significant gaps in the knowledge in this area,[71−77] we will refrain from making assumptions, and instead we report formation energies according to conventional point defect chemistry, which can be corroborated in laboratory conditions through conventional synthesis and doping strategies.

The binding energy E_b of a defect cluster is defined as the energy released (or absorbed) to form a bound cluster from the constituent defects in dilute form. For instance, considering the following trivacancy cluster, in Kröger−Vink notation,[78]

$$V_C + 2V_W \rightarrow \{V_C{:}V_W{:}V_W\}$$

the binding energy is defined as

$$E_b(\{V_C{:}V_W{:}V_W\}) = E_f(\{V_C{:}V_W{:}V_W\}) - E_f(V_C) - 2E_f(V_W)$$

thus a negative E_b implies an attractive interaction and positive E_b implies a repulsive interaction. Note that the binding energy is insensitive to the definition of chemical potential, as all the μ_x terms cancel out. We use the following short-hand notation to define larger clusters: $V_{jkl} = \{V_j{:}V_k{:}V_l\}$.

The binding energy of clusters containing more than two defects may be described as the sum of the pairwise defect−defect interaction plus a many-body term. Taking for instance a vacancy triplet, the binding energy may be described as[79]

$$E_b(V_{klm}) = E_b(V_{kl}) + E_b(V_{lm}) + E_b(V_{mk}) + E_{\text{three-body}}$$

$$E_b(V_{klm}) = \sum_{i\neq j}^{n} E_b(V_{ij}) + E_{\text{three-body}}$$

where $E_b(V_{jkl})$ is the DFT-calculated binding energy of the vacancy triplet, $E_b(V_{ij})$ is the DFT-calculated binding energy of vacancy pair (ij) with same the same configuration as that found in the vacancy triplet (three pair configurations), and $E_{\text{three-body}}$ is defined as the energy difference (positive or negative) between the explicitly calculated binding energy and the sum of the pairwise interactions.

More generally, for a cluster containing n vacancy this is expanded as

$$E_b(V_1{:}V_2{:}\ldots{:}V_n) = E_{\text{pairwise}} + (E_{\text{three-body}} + E_{\text{four-body}} + \ldots)$$

$$E_b(V_1{:}V_2{:}\ldots{:}V_n) = \sum_{i\neq j}^{n} E_b(V_{ij}) + E_{\text{many-body}}$$

This definition allows for an estimation of the binding energy of a cluster of arbitrary size from the binding energy of a cluster of smaller sizes.

3. VACANCY CLUSTERS

Defect clustering is the first step in the microstructural evolution of materials exposed to radiation. For instance, vacancy clustering may lead to void nucleation, the formation of (vacancy) dislocation loops, and decreased vacancy-mediated solute diffusion and self-diffusion. In this section we investigate the formation of vacancy clusters, starting from divacancies and then considering larger vacancy clusters.

DOI: 10.1021/acsaem.9b01990
ACS Appl. Energy Mater. 2020, 3, 868−878

Divacancy clusters made up of either two C vacancies {V_C:V_C}, two tungsten vacancies {V_W:V_W}, or a Schottky pair {V_C:V_W} were considered. Henceforth, these clusters will be referred to as V_{CC}, V_{WW}, and V_{CW}, respectively. For each cluster type, we simulated all divacancy configurations with interdefect distance ranging from first nearest neighbor (1nn) to twelfth nearest neighbor (12nn), as illustrated in Figure 1. Table 2 provides the nomenclature used to uniquely identify defect clusters, as a function of nearest neighbor distances.

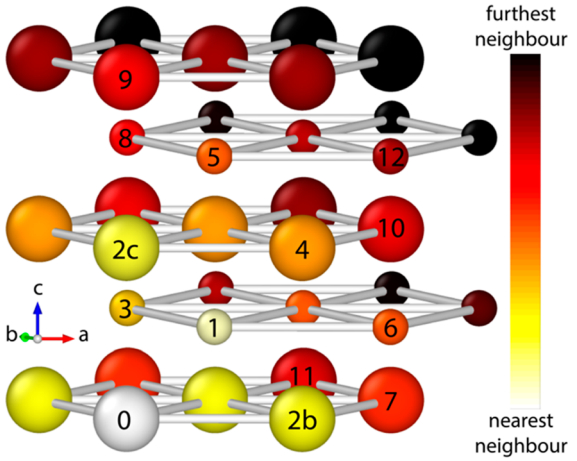

Figure 1. WC lattice where large and small spheres represent W and C, respectively. Atoms color-coded according to the distance from atom 0, and labeled according to nomenclature of Table 2. Note that W and C occupy symmetrically equivalent sublattices.

Table 2. W−W, C−C, and W−C Nearest Neighbor Distances[a]

nearest neighbor	distance (Å)	multiplicity	sublattice
1	2.20	6	opposite
2c	2.84	2	same
2b	2.91	6	same
3	3.65	6	opposite
4	4.07	12	same
5	4.58	6	opposite
6	4.67	12	opposite
7	5.04	6	same
8	5.43	6	opposite
9	5.69	2	same
10	5.79	12	same
11	5.82	6	same
12	6.16	12	opposite

[a]The last column specifies whether the two defects reside on the same sublattice or on opposite sublattices. The two sublattices are equivalent.

The binding energies of the divacancy clusters are presented in Figure 2. All V_{CW} exhibit negative (favorable) binding energy, with a remarkably strong binding in the first nearest neighbor configuration (−1.38 eV). This suggests that dissimilar vacancies exhibit an attractive force and will tend to form bound Schottky defects where the two vacancies are nearest neighbors. V_{WW} also exhibits significant binding in all but one configuration (9th nn), with the most favorable configurations observed at the closest nearest neighbors (2c and 2b configurations). On the other hand, V_{CC} clusters exhibit positive binding energies throughout, indicating that

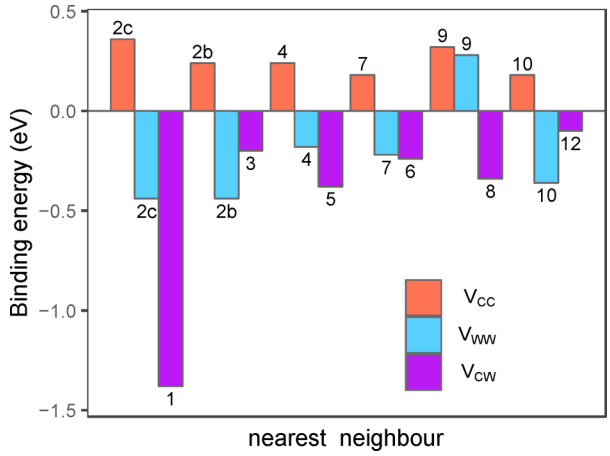

Figure 2. Binding energies of divacancy clusters.

there is a clear repulsion between C vacancies, and that no carbon vacancy clusters will form unless tungsten vacancies are present.

Given the strong binding observed in some divacancy clusters, we also considered trivacancy and tetravacancy clusters. To reduce the large number of possible three-body and four-body configurations into a computationally practicable number of simulations, we considered only those clusters where at least one pair of vacancies was in the most favorable configuration for a divacancy cluster of that type. By way of example, Figure 3a shows three V_{CCW} clusters where the

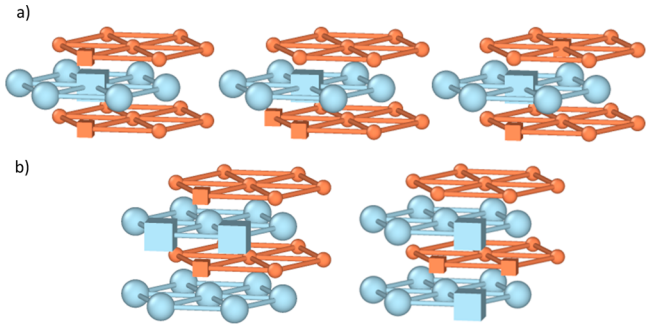

Figure 3. (a) Configuration of the most stable trivacancy cluster V_{CCW}. Equivalent arrangements were used for V_{CWW} clusters. (b) Configuration of most stable tetra-vacancy clusters V_{CCWW}. Boxes represent vacant sites.

strongly bound V_{CW}−1nn cluster is observed twice for each configuration. Figure 3b shows two V_{CCWW} clusters where the same V_{CW}−1nn interaction appears four times, as well as the favorable V_{WW}−2nn interactions. Overall, we considered 14 trivacancy configurations and 25 tetravacancy configurations.

Figure 4 shows the per-vacancy formation energy (top) and binding energy (bottom) of vacancy clusters as a function of the clusters composition. The results are also illustrated as a function of cluster size in the Supporting Information, together with tabulated data.

Figure 4 (top) shows a clear trend of increasing stability with increasing concentration of carbon vacancies in the cluster. V_C-rich clusters exhibit lower formation energy per vacancy than V_W-rich clusters, with cluster size affecting the energy only to the second order (detailed description of the effect of cluster size on formation energy of clusters is provided in the

DOI: 10.1021/acsaem.9b01990
ACS Appl. Energy Mater. 2020, 3, 868−878

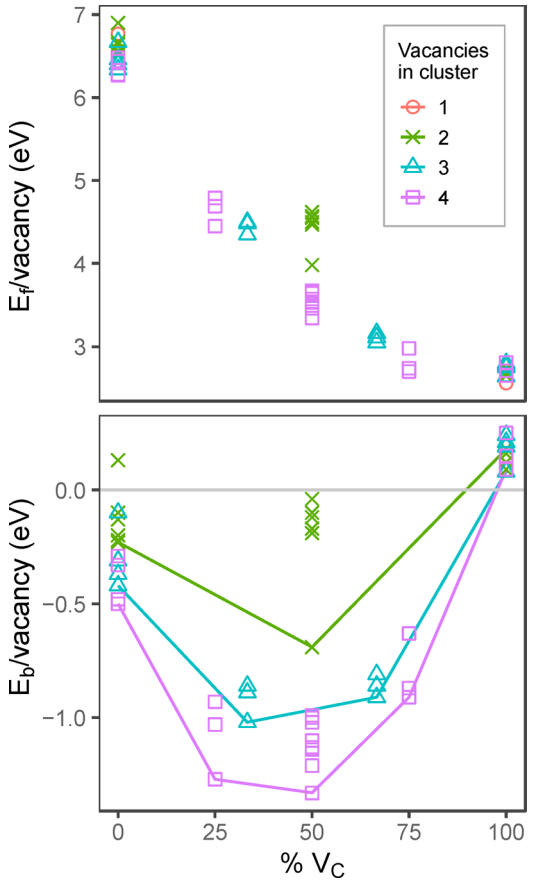

Figure 4. Formation energy (top) and binding energy (bottom) of vacancy clusters, color-coded by cluster size. Lines outline the convex hull for each cluster size.

Supporting Information Figure S1). This suggest that carbon vacancies are more easily accommodated in the lattice than tungsten vacancies, irrespective of whether they form clusters or remain dilute.

On the other hand, mixed V_C−V_W clusters appear to be strongly bound, Figure 4 (bottom), reaching binding energies of −1.33 eV/vacancy when the cluster is composed of an equal number of V_C and V_W (i.e., $V_C/(V_C + V_W) = 0.5$). Any deviation from this cluster stoichiometry leads to a decrease in cluster stability (reduced binding). The attractive binding energy of mixed V_C−V_W clusters appears to increase with increasing cluster size, within the clusters considered here. For both trivacancy and tetravacancy clusters, the most favorable clusters are composed of a mixture of V_C and V_W, arranged in the most compact configurations (shown in Figure 3). These cluster configurations are the ones where the strongly bound V_{CW}−1nn pairwise interaction is present multiple times. However, all other V_{CCWW} mixed cluster configurations (i.e., tetravacancies with equal portion of C and W vacancies) are also strongly bound.

Although pure V_C clusters exhibit the lowest formation energies (~2.5 eV/vacancy), they also have the largest repulsive (positive) binding energies. This indicates that single C vacancies will be accommodated in dilute form and will not cluster unless associated with one or more W vacancies. On the other hand, dilute W vacancy clusters are not readily accommodated in WC, but their formation energy can be greatly reduced by clustering with C vacancies. Generally, all clusters will tend to have equal number of C and W vacancies, owing to the highly favorable $\{V_C{:}V_W\}$−1nn pairwise interaction.

It is likely that the trend in our data would continue for larger vacancy clusters, but these are too large to be modeled explicitly with the current method. We have therefore used the defect energies of the vacancy pairs to approximate the binding energy of larger clusters with the assumption that the pairwise interactions dominate over many-body interactions. Figure 5

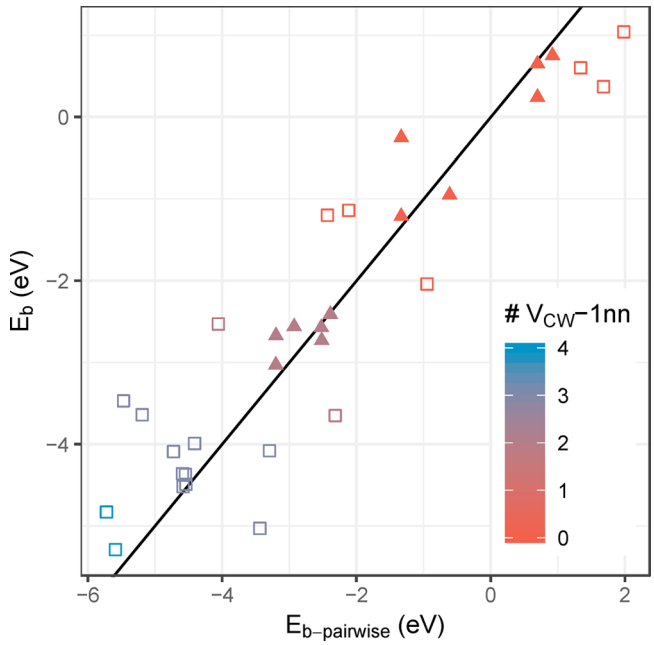

Figure 5. Binding energy of trivacancy (triangle) and tetravacancy (squares) clusters, as a function of the pairwise component of the total binding energy. Color coded by the number of $\{V_C{:}V_W\}$−1nn pairwise interactions. Black line indicates perfect match (E_b = $E_{pairwise}$).

shows that the pairwise interactions provide a reasonable first-order approximation for the binding energy of trivacancy clusters (filled triangles), and less so for tetra-vacancy clusters (hollow squares). The accuracy of this method is clearly insufficient to make a quantitative prediction for larger clusters, but nevertheless the trend of increasing binding energy for clusters containing a majority of $\{V_C{:}V_W\}$−1nn pairwise interactions is evident (i.e., blue data points are consistently lower energy than red ones), reinforcing the finding that larger vacancy clusters containing a similar number of V_C and V_W are likely to form.

4. INTRINSIC DISORDER PROCESSES

Disorder processes in WC have been investigated in previous literature[20,54] within the common approximation that all defect concentrations are in the dilute, noninteracting limit. In light of the remarkable stability of vacancy clusters presented above, we re-examined the disorder processes to include defect clusters as well as dilute defects.

To that end, a similar analysis presented above for vacancy clusters was repeated for antisite clusters $\{C_W{:}C_W\}$, $\{W_C{:}W_C\}$ and bound antisite $\{C_W{:}W_C\}$. These were found to exhibit strongly attractive binding energy, as large as −15.46 eV in the case of $\{C_W{:}W_C\}$, which exhibits opposing strain field (refer to the Supporting Information for detailed list of defect energies).

DOI: 10.1021/acsaem.9b01990
ACS Appl. Energy Mater. 2020, 3, 868−878

Substitution-interstitial pairs were also investigated, as these configurations were observed to form spontaneously as a result of atomic relaxation from unstable tungsten interstitials. All $\{W_C:C_i\}-1nn$ clusters were considered, and three configurations were found to be stable exhibiting attractive large binding energies ranging from −5.80 eV to −8.14 eV (refer to the Supporting Information for full list of defect energies). As both W_C and C_i create compressive strain fields, minimizing elastic strain is not the sole driving force for defect clustering in WC.

Table 3 shows the energy associated with Frenkel, Schottky, and antisite disorder, calculated with both the conventional assumption of dilute noninteracting point defects, and from the formation energy of bound defect pairs. Where more than one configuration exists (e.g., multiple stable interstitial sites, or multiple nonequivalent clusters of the same composition) the range of energy is provided, with the lowest energy value being the most relevant near equilibrium.

Table 3. − Energies of antisite, Schottky, and Frenkel disorder processes[a]

	formation energy (eV)	
disorder process	dilute	clustered
antisite	22.30	6.84−11.16
Schottky	9.34	6.70−9.25
C-Frenkel	7.09−10.36	
W-Frenkel	21.08−25.82	

[a]These are the total reaction energy to accommodate the process, thus the formation energy of the individual defects involved in these processes is half of the value reported in this table (all processes involve only two defects).

It is evident that clustered configurations significantly reduce the energy required to accommodate disorder in WC. The reduction in energy is particularly remarkable for antisite pair production, which appeared to be the least likely mechanisms under dilute conditions and is found to be highly favorable when clusters are considered. Similarly, Schottky pairs exhibit a remarkable reduction in formation energy when forming clusters, as was shown in Figure 4.

Frenkel pairs are also expected to exhibit a reduction in energy at high concentration (small defect distances), however, clusters of these were not calculated because (a) at the first and second nearest neighbor, the defects are expected to annihilate spontaneously and (b) at larger distances the number of vacancy−interstitial combinations are computationally intractable.

Overall, the large formation energies of W-Frenkels (21.08−25.82 eV) indicate that this disorder process is negligible under equilibrium conditions. On the other hand, bound Schottky, bound antisite, and C-Frenkel defects have much lower formation energies of 6.70, 6.84, and 7.09 eV, respectively. All three processes are likely to compete in the accommodation of disorder in the material, under both equilibrium and nonequilibrium conditions (e.g., radiation damage). The findings are in qualitative agreement with positron lifetime spectroscopy measurements of WC,[27] which observe that only C vacancies are formed following irradiation with 1 MeV electrons (at 200 K with a dose of 1.8×10^{23} m^{-2}), but both W and C vacancies are observed in samples irradiated with 2.5 MeV electrons (at 80 K with a dose of 1.2×10^{22} m^{-2}). In all cases, the predominant defects show a strong tendency to cluster, indicating that at the elevated temperatures of operations in a fusion reactor, the defects are likely to evolve into extended defects, such as dislocation loops and voids.

5. ACCOMMODATION OF TRANSMUTATION PRODUCTS TA, RE, AND OS

Exposure to neutron fluxes causes activation and transmutation of W. Among the many decay products, tantalum (Ta), rhenium (Re), and osmium (Os) have been shown to form in considerable amounts.[13] These elements are known to deteriorate the mechanical properties of metallic W,[45−52] and it is therefore important to investigate their interaction and redistribution within WC.

Given the chemical affinity with W, and the similar metallic radii, it is reasonable to assume that Ta, Re, and Os will most likely be accommodated on W sites. Nevertheless, all possible interstitial sites were also considered, and five stable interstitial sites were found for each element. The calculated formation energies for solution from the standard state (metallic Ta, Re, and Os) and from monocarbides (TaC, ReC, and OsC) are shown in Table 4. As expected, all three elements are most easily accommodated as substitutions on W sites. All dilute interstitial defects exhibit large formation energies of similar magnitude to W_i, with the TriC site being the most favorable, as is the case for W self-interstitials.

Table 4. − Formation Energies of Ta, Re, and Os Defects from Standard State. In Brackets, The Corresponding Solution Energies from XC (X = Ta, Re, Os)

defect	Ta	Re	Os
X_W	−0.08 (0.81)	0.16 (−0.58)	1.05 (−0.77)
X_i (TriC)	15.32	13.14	12.58
X_i (TriW)	15.77	16.04	16.48
X_i (HexW)	19.10	15.65	17.92
X_i (a-Crowdion)	15.77	15.92	16.13
X_i (c-Crowdion)	17.56	17.43	17.79

Once transmutation products form, they may be retained in the WC lattice, or they may precipitate out as a secondary phase. The competition between dissolution and precipitation can be predicted by considering the formation energy of the defects and that of the competing precipitate phases. In the case of Ta, it is reasonable to assume that TaC (NaCl structure) is the most likely competing phase.[71−73] On the other hand, limited thermodynamic information is available regarding the WC region of C−Re−W and C−Os−W phase diagrams.[74−77] ReC and OsC phases have been reported experimentally, but only at high-pressures,[80,81] while Re_2C has also been reported as a stable competing phase for accommodation of Re. Some phase diagrams show that the competing phases are the elemental metals Re and Os, or their solid solution phase with W metal, but this is extrapolated from limited thermodynamic data, and the formation of ternary phases cannot be excluded definitively. Additionally, the stability of the potential phases would be strongly sensitive to the stoichiometry variation of WC.

The positive solution energy of TaC (0.81 eV) indicates that Ta exhibits limited solubility in WC and will preferentially segregate as cubic TaC instead. If one were to assume that ReC and OsC are the most likely phases competing against solubility, it would appear that Re and Os are highly soluble in WC. However, that is not the case if one considers the

DOI: 10.1021/acsaem.9b01990
ACS Appl. Energy Mater. 2020, 3, 868−878

formation of metallic Re and Os instead. This in itself is a further indication that ReC and OsC are most likely not the thermodynamically competing phases in Re- and Os-doped WC. Taking the elemental metals Re and Os as the best representation of the true competing phase, it appears that Re exhibits some (limited) solubility in WC, especially at high temperatures (E_{sol} = 0.16 eV), while Os exhibits significantly lower solubility in WC (E_{sol} = 1.05 eV), with a strong drive for segregation. The formation of Os-rich precipitate may also influence the thermodynamic of Ta and Re accommodation in WC, by providing an alternative competing phase in which these elements may dissolve.

These results only consider dilute, binary mixtures. To investigate the effect of increasing concentration beyond the dilute noninteracting regime, we simulated clusters containing multiple transmutation elements. All possible configurations of disubstitution clusters onto W sites were simulated up to the 10th nearest neighbor (here we are also counting C atoms in the neighbor list, consistent with Figure 1 and Table 2). The resulting binding energies are shown in Figure 6 (tabulated values in Supporting Information).

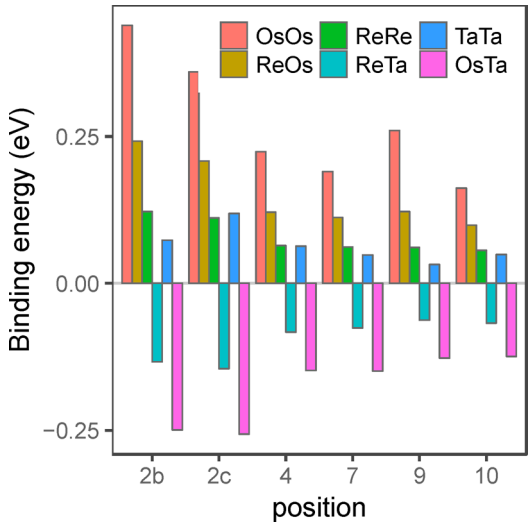

Figure 6. Binding energy of clusters comprising Ta, Re, and Os transmutation elements on W sites.

In most cases, the binding energy between defect pairs is positive (i.e., repulsive), with the notable exceptions of Re−Ta and Os−Ta clusters. These defect pairs exhibit an attraction at all distances considered here, with increasing strength at closer distance. It is therefore expected that Ta will be colocated with Re and Os when in solution in WC.

We have also considered the potential binding of transmutation elements with intrinsic defects caused by radiation damage, specifically W and C vacancies, presented in Figure 7. All three transmutation elements considered here show some degree of binding toward W vacancies (bottom panel). These generally increase with increasing proximity to the W vacancy, and the binding is strongest for Os. At the closest distance, the in-plane configuration (2b) is preferred by Os and Re, while the *c*-axis aligned configuration (2c) is preferred by Ta. Favorable binding energies of $\{Ta_W/Re_W/Os_W{:}V_W\}$ clusters suggest that the presence of transmutation elements may stabilize W vacancies, thereby potentially accelerating radiation-induced swelling in the material. On the other

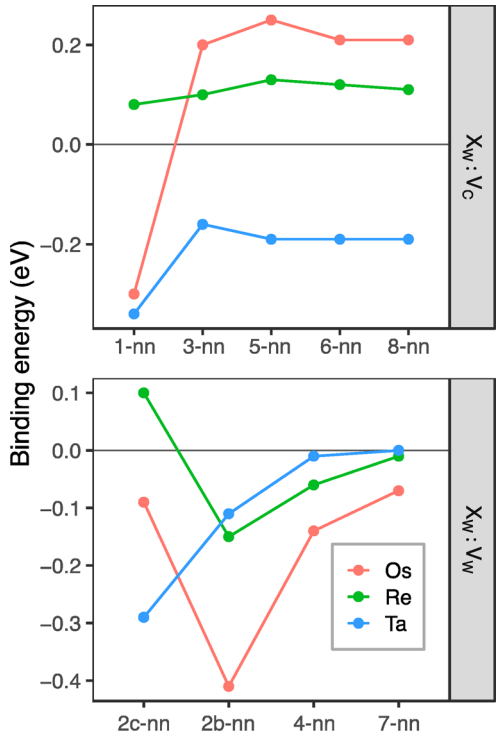

Figure 7. − Binding energy of Ta/Re/Os substitutions with a C vacancy (top) and a W vacancy (bottom), as a function of nearest neighbor distance between substitution and vacancy.

hand, Os and Re show clear repulsion from C vacancies (except for the $\{Os_W{:}V_C\}$−1nn cluster), while Ta exhibits attraction to C vacancies at all distances. Given that W and C vacancies are also strongly bound (see section 3), this suggests that vacancy clusters and voids will likely be decorated by Ta, and possibly also by Re and Os.

The favorable binding between Ta_W and Os_W and Re_W also has a stabilizing effect on the constituent defects: it implies that the coproduction of Ta together with Re and Os leads to a slight increase in solubility limit of the constituent elements, by reducing the associated solution energy by up to 0.07−0.13 eV/atom. This is, however, a comparatively small change compared to the solution energy of Ta Re and Os in WC. This can be clearly seen in Figure 8 (irrespective of which reference phase is considered), where the solution energy of pairs of dopants (e.g., Re+Ta) appears to be only slightly less than the average of the solution energy of their respective constituents (e.g., Re and Ta in isolation).

In Figure 8 the solution energies are calculated taking into account both dilute and pair cluster defects. The top two panels consider the case where the competing phase for precipitation are the elemental metals (top) or their respective monocarbides (middle). It is evident that the predicted solubility is strongly sensitive to the choice of reference phase. The bottom panel of Figure 8 presents the case where the competing phases for precipitation are taken as TaC, $Re_{(s)}$, and $Os_{(s)}$. According to the best available experimental thermodynamic data of the C−(Ta,Re,Os)−W ternary phase, these are the most relevant phases that may precipitate in the presence of Ta, Re, and Os in WC.[71−77] In this scenario, all elements exhibit limited solubility and are predicted to segregate. This is further confirmed by considering solution enthalpies at 300 K, extrapolated to any arbitrary cluster

DOI: 10.1021/acsaem.9b01990
ACS Appl. Energy Mater. 2020, 3, 868−878

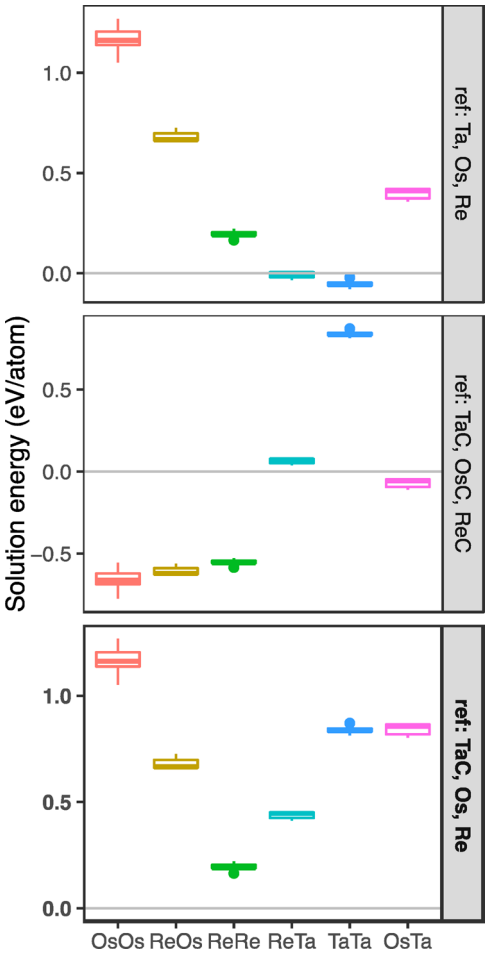

Figure 8. Solution energies of the transmutation elements from dilute point defects and binary clusters, assuming that the thermodynamically competing phases are (top) the elemental metals $Ta_{(s)}$, $Re_{(s)}$, and $Os_{(s)}$; (middle) their monocarbides TaC, ReC, OsC, and (bottom) the most likely phases according to the limited experimental thermodynamic information available on ternary C−X−W systems (see text).

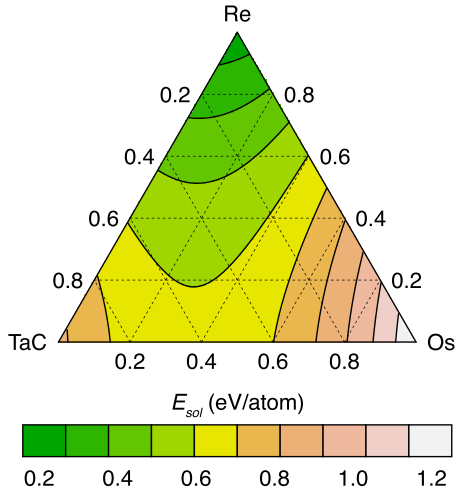

Figure 9. Enthalpy of solution (at 300 K) of TaC, Re, and Os transmutation elements in WC as a function of impurity composition. Interpolation in ternary space was performed exclusively from binary and unary data.

composition, presented in Figure 9. These are obtained by considering all dilute and clustered defects, and averaging the formation enthalpies following Boltzmann statistics. The Supporting Information contains similar plots produced at 0, 300, and 2000 K, and with respect to different competing phases for precipitation (Ta/Os/Re, TaC/ReC/OsC, and TaC/Re/Os).

In short, it is predicted that the most common activation products of W formed by irradiation with fusion neutrons are largely insoluble in WC under equilibrium conditions. However, the formation or Re−Ta and Os−Ta clusters appears to slightly increase the solubility of the cogenerated transmutation products; and the binding of W vacancies to Ta/Re/Os, and that of C vacancies to Ta, suggest that the excess vacancies caused by radiation damage will be stabilized by the transmutation of W into Ta, Re, and Os, and that vacancy defects (voids, dislocation loops) will be enriched in transmutation elements.

It is important bear in mind that shielding material in fusion tokamaks are subject to conditions that are far from equilibrium (continued exposure to a fast neutron flux, strong temperature gradients, and potentially fast temperature transitions), and therefore there is no guarantee that the solutes will partition according to the thermodynamic solubility regimes. For instance, it has been observed that neutron irradiation of W metal at temperatures below 800 °C leads to the formation of Os−Re precipitates at fluences higher than 1.5 dpa, even when the solute concentration is below the thermodynamic solubility limit.[48] Whether or not a behavior similar to that observed in W can be expected in WC depends on many factors, not the least what are the most likely competing phases for segregation, for which there is a clear lack of both experimental and computational knowledge, and further investigation in this area is encouraged. An additional consideration that should be taken into account, beyond the thermodynamic insight into phase stability and interfacial energies, is the kinetic drag of solutes toward defect sinks such as grain boundaries, which could lead to local enrichment/depletion of solutes at microstructural features, beyond/below the solubility limits.

6. CONCLUSIONS

Deviation of stoichiometry in WC is entirely accommodated by C vacancy (WC_{1-x}) and C interstitials (WC_{1+x}), as these are the most energetically favorable dilute point defects. At higher concentrations, vacancy clusters containing at least one V_W exhibit significant drive toward clustering. Particularly strong binding was observed for mixed vacancy clusters V_{CW}, V_{CCW}, V_{CWW}, and V_{CCWW}, with no indication that the trend toward binding would decrease in larger clusters. The favorable clustering of vacancies suggests that void nucleation may be a concern in WC.

Almost all substitution clusters and antisites were found to have favorable binding energies. In particular, the 1nn antisite $\{C_W{:}W_C\}$ exhibited remarkably strong binding, reducing the overall formation energy of an antisite pair from 22.30 eV for dilute defects, to 6.84 eV. Clusters involving an antisite with an interstitial yielded similar results, indicating that these types of defect will also readily form clusters in WC.

With regard to disorder processes, bound Schottky, bound antisites, and C-Frenkel showed lower formation energies of 6.70, 6.84, and 7.09 eV, respectively. All three processes will compete in the accommodation of disorder in the material,

DOI: 10.1021/acsaem.9b01990
ACS Appl. Energy Mater. 2020, 3, 868−878

providing multiple pathways for microstructural evolution induced by radiation damage. In the case of Schottky and antisite processes, this will lead to the formation of defect clusters, which may grow into extended defects (e.g., dislocation loops and voids).

The accommodation of Ta, Re, and Os transmutation products in WC is achieved entirely by substitution onto the W sublattice, while interstitial defects appear highly unfavorable, with similar defect energies to W self-interstitials. The solubility of Ta, Re, and Os in WC is likely very limited, however accurate prediction requires more thermodynamic information on the C−(Ta,Re,Os)−W phase diagram, which is currently scarce. An in-depth analysis of the WC−corner of the ternary−quaternary and quinary phase diagrams is encouraged, similar to that done on the C−V−W system.[82]

Re and Os are expected to cluster with W vacancies, and Ta will bind with both W and C vacancies. Thus, voids and vacancy loops will likely be enriched in Ta, Re, and Os. The formation of these clusters may further stabilize the intrinsic vacancies and lead to accelerated swelling in the material. This deleterious effect may be mitigated by encouraging the partitioning of transmutation elements into secondary phases; however, this must be balanced against the potentially negative effect of precipitating secondary phases.

Overall, the findings of this study do not rule out WC as a candidate material for shielding of spherical tokamak fusion reactors. However, further investigation is required to assess the nature of extended defects that may form as a result of radiation damage, and their impact on the materials properties. The possibility of exploiting the anisotropic diffusion character of WC via texture engineering could be explored as a potential avenue to mitigate the adverse microstructural evolution revealed in this paper.

■ ASSOCIATED CONTENT

Supporting Information

The Supporting Information is available free of charge at https://pubs.acs.org/doi/10.1021/acsaem.9b01990.

Additional results including calculated bulk properties of WC and comparison with literature, tabulated formation and binding energies for all the clusters considered in this study, and predicted solution energies of Ta, TaC, Re, ReC, Os, and OsC at 0, 300, and 2000 K (PDF)

■ AUTHOR INFORMATION

Corresponding Author

*E-mail: p.burr@unsw.edu.au.

ORCID

Samuel X. Oliver: 0000-0001-9521-7533

Patrick A. Burr: 0000-0003-4796-9110

Notes

The authors declare no competing financial interest.

■ ACKNOWLEDGMENTS

P.A.B. acknowledges the Tyree Foundation and the Australian Nuclear Science and Technology Organisation for financial support. This research was undertaken with the assistance of resources and services from the National Computational Infrastructure (NCI), the Multimodal Australian ScienceS Imaging and Visualisation Environment (MASSIVE), and the Pawsey Supercomputing Centre, all of which are supported by Australian Federal and State Governments.

■ REFERENCES

(1) Costley, A. E. Towards a compact spherical tokamak fusion pilot plant. *Philos. Trans. R. Soc., A* **2019**, *377*, 20170439.

(2) Humphry-Baker, S. A.; Smith, G. D. W. Shielding materials in the compact spherical tokamak. *Philos. Trans. R. Soc., A* **2019**, *377*, 20170443.

(3) Frischherz, M. C.; Kirk, M. A.; Farmer, J.; Greenwood, L. R.; Weber, H. W. Defect cascades produced by neutron irradiation in YBa2Cu3O7−*δ*. *Phys. C* **1994**, *232* (3−4), 309−327.

(4) Sears, V. F. Neutron Scattering Lengths and Cross Sections. *Neutron News* **1992**, *3* (3), 26−37.

(5) Windsor, C. G.; Marshall, J. M.; Morgan, J. G.; Fair, J.; Smith, G. D. W.; Rajczyk-Wryk, A.; Tarragó, J. M. Design of cemented tungsten carbide and boride-containing shields for a fusion power plant. *Nucl. Fusion* **2018**, *58* (7), 076014.

(6) Humphry-Baker, S. A.; Harrison, R. W.; Greaves, G.; Knowles, A. J.; Smith, G. D. W.; Donnelly, S. E.; Lee, W. E. A candidate fusion engineering material, WC-FeCr. *Scr. Mater.* **2018**, *155*, 129−133.

(7) Humphry-Baker, S. A.; Lee, W. E.. Oxidation resistant coating and methods of manufacturing thereof. WO Patent WO2017168147A1, 2017.

(8) Kingham, D.; Smith, G.. Shielding materials for fusion reactors. WO Patent WO2016009176A1, 2016.

(9) Tejado, E.; Dias, M.; Correia, J. B.; Palacios, T.; Carvalho, P. A.; Alves, E.; Pastor, J. Y. New WC-Cu thermal barriers for fusion applications: High temperature mechanical behaviour. *J. Nucl. Mater.* **2018**, *498*, 355−361.

(10) Dias, M.; Guerreiro, F.; Tejado, E.; Correia, J. B.; Mardolcar, U. V.; Coelho, M.; Palacios, T.; Pastor, J. Y.; Carvalho, P. A.; Alves, E. WC-Cu thermal barriers for fusion applications. *Surf. Coat. Technol.* **2018**, *355* (2017), 222−226.

(11) Humphry-Baker, S. A.; Smith, G. D. W.; Pintsuk, G. Thermal shock of tungsten carbide in plasma-facing conditions. *J. Nucl. Mater.* **2019**, *524*, 239−246.

(12) Fang, Z. Z.; Wang, X.; Ryu, T.; Hwang, K. S.; Sohn, H. Y. Synthesis, sintering, and mechanical properties of nanocrystalline cemented tungsten carbide - A review. *Int. J. Refract. Hard Met.* **2009**, *27* (2), 288−299.

(13) Gilbert, M. R.; Sublet, J.-C. Neutron-induced transmutation effects in W and W-alloys in a fusion environment. *Nucl. Fusion* **2011**, *51* (4), No. 043005.

(14) Humphry-Baker, S. A.; Peng, K.; Lee, W. E. Oxidation resistant tungsten carbide hardmetals. *Int. J. Refract. Hard Met.* **2017**, *66*, 135−143.

(15) Liu, K.; Li, X. P. Ductile cutting of tungsten carbide. *J. Mater. Process. Technol.* **2001**, *113* (1−3), 348−354.

(16) Lee, M.; Gilmore, R. S. Single crystal elastic constants of tungsten monocarbide. *J. Mater. Sci.* **1982**, *17* (9), 2657−2660.

(17) Sara, R. V. Phase Equilibria in the System Tungsten—Carbon. *J. Am. Ceram. Soc.* **1965**, *48* (5), 251−257.

(18) Humphry-Baker, S. A.; Lee, W. E. Tungsten carbide is more oxidation resistant than tungsten when processed to full density. *Scr. Mater.* **2016**, *116*, 67−70.

(19) Humphry-Baker, S. A. Unpublished measurement of thermal transport in WC. *Personal Communication*, 2019.

(20) Burr, P. A.; Oliver, S. X. Formation and migration of point defects in tungsten carbide: Unveiling the sluggish bulk self-diffusivity of WC. *J. Eur. Ceram. Soc.* **2019**, *39* (2−3), 165−172.

(21) Ang, C.; Silva, C.; Shih, C.; Koyanagi, T.; Katoh, Y.; Zinkle, S. J. Anisotropic swelling and microcracking of neutron irradiated Ti3AlC2-Ti5Al2C3 materials. *Scr. Mater.* **2016**, *114*, 74−78.

(22) Ang, C.; Zinkle, S.; Shih, C.; Silva, C.; Cetiner, N.; Katoh, Y. Phase stability, swelling, microstructure and strength of Ti3SiC2-TiC ceramics after low dose neutron irradiation. *J. Nucl. Mater.* **2017**, *483*, 44−53.

DOI: 10.1021/acsaem.9b01990
ACS Appl. Energy Mater. 2020, 3, 868−878

(23) Snead, L. L.; Zinkle, S. J. Use of beryllium and beryllium oxide in space reactors. *AIP Conf. Proc.* **2005**, *746*, 768−775.
(24) Fremlin, J. H.; Askouri, N. A. Hardening of tungsten carbide by irradiation. *Nature* **1974**, *249*, 137.
(25) Askouri, N. A.; Fremlin, J. H. Hardening of tungsten carbide tools by charged particle irradiation. *Met. Technol.* **1975**, *2*, 538−541.
(26) Hershkowitz, N.; Wender, S. A.; Oberley, L. W. Radiation damage in tungsten carbide. *Phys. Lett. A* **1970**, *33*, 89−90.
(27) Rempel, A.; Würschum, R.; Schaefer, H.-E. Atomic defects in hexagonal tungsten carbide studied by positron annihilation. *Phys. Rev. B: Condens. Matter Mater. Phys.* **2000**, *61*, 5945−5948.
(28) Chen, Z.; Han, W.; Yu, J.; Zhu, K. Effect of 800 keV argon ions pre-damage on the helium blister formation of tungsten exposed to 60 keV helium ions. *J. Nucl. Mater.* **2016**, *472*, 110−117.
(29) Ueda, Y.; Peng, H. Y.; Lee, H. T.; Ohno, N.; Kajita, S.; Yoshida, N.; Doerner, R.; De Temmerman, G.; Alimov, V.; Wright, G. Helium effects on tungsten surface morphology and deuterium retention. *J. Nucl. Mater.* **2013**, *442* (1−3SUPPL.1), S267−S272.
(30) Cui, M.H.; Shen, T.L.; Zhu, H.P.; Wang, J.; Cao, X.Z.; Zhang, P.; Pang, L.L.; Yao, C.F.; Wei, K.F.; Zhu, Y.B.; Li, B.S.; Sun, J.R.; Gao, N.; Gao, X.; Zhang, H.P.; Sheng, Y.B.; Chang, H.L.; He, W.H.; Wang, Z.G. Vacancy like defects and hardening of tungsten under irradiation with He ions at 800 °C. *Fusion Eng. Des.* **2017**, *121*, 313−318.
(31) Garrison, L. M.; Kulcinski, G. L. Effects of 30 keV helium irradiation on (110) single crystal tungsten. *Fusion Sci. Technol.* **2013**, *64*, 216−220.
(32) Meyer, F. W.; Hijazi, H.; Bannister, M. E.; Unocic, K. A.; Garrison, L. M.; Parish, C. M. Flux threshold measurements of He-ion beam induced nanofuzz formation on hot tungsten surfaces. *Phys. Scr.* **2016**, *T167*, 014019−014026.
(33) Fan, H.; Endo, T.; Bi, Z.; Yan, W.; Ohnuki, S.; Yang, Q.; Ni, W.; Liu, D. Current mapping of low-energy (120 eV) helium and hydrogen irradiated tungsten by conductive atomic force microscopy. *J. Nucl. Mater.* **2017**, *486*, 191−196.
(34) Ryabtsev, S.; Gasparyan, Y.; Zibrov, M.; Shubina, A.; Pisarev, A. Deuterium thermal desorption from vacancy clusters in tungsten. *Nucl. Instrum. Methods Phys. Res., Sect. B* **2016**, *382*, 101−104.
(35) Gavish Segev, I.; Yahel, E.; Silverman, I.; Makov, G. Blister formation at subcritical doses in tungsten irradiated by MeV protons. *J. Nucl. Mater.* **2017**, *496*, 77−84.
(36) Chen, W. Q.; Xiao, X. Z.; Pang, B.; Si, S. S.; Jia, Y. Z.; Xu, B.; Morgan, T. W.; Liu, W.; Chiu, Y. L. Irradiation hardening induced by blistering in tungsten due to low-energy high flux hydrogen plasma exposure. *J. Nucl. Mater.* **2019**, *522*, 11−18.
(37) Wang, Z.; Wang, J.; Yuan, Y.; Cheng, L.; Qin, S.-Y.; Kreter, A.; Lu, G.-H. Effects of tantalum alloying on surface morphology and deuterium retention in tungsten exposed to deuterium plasma. *J. Nucl. Mater.* **2019**, *522*, 80−85.
(38) Zhang, Z. X.; Chen, D. S.; Han, W. T.; Kimura, A. Irradiation hardening in pure tungsten before and after recrystallization. *Fusion Eng. Des.* **2015**, *98*−*99*, 2103−2107.
(39) Yi, X.; Jenkins, M. L.; Kirk, M. A.; Zhou, Z.; Roberts, S. G. In-situ TEM studies of 150 keV W+ ion irradiated W and W-alloys: Damage production and microstructural evolution. *Acta Mater.* **2016**, *112*, 105−120.
(40) Založnik, A.; Markelj, S.; Schwarz-Selinger, T.; Schmid, K. Deuterium atom loading of self-damaged tungsten at different sample temperatures. *J. Nucl. Mater.* **2017**, *496*, 1−8.
(41) Simmonds, M. J.; Wang, Y. Q.; Barton, J. L.; Baldwin, M. J.; Yu, J. H.; Doerner, R. P.; Tynan, G. R. Reduced deuterium retention in simultaneously damaged and annealed tungsten. *J. Nucl. Mater.* **2017**, *494*, 67−71.
(42) Zhang, Z.; Yabuuchi, K.; Kimura, A. Defect distribution in ion-irradiated pure tungsten at different temperatures. *J. Nucl. Mater.* **2016**, *480*, 207−215.
(43) Markina, E.; Mayer, M.; Manhard, A.; Schwarz-Selinger, T. Recovery temperatures of defects in tungsten created by self-implantation. *J. Nucl. Mater.* **2015**, *463*, 329−332.
(44) Shimada, M.; Oya, Y.; Wampler, W. R.; Yamauchi, Y.; Taylor, C. N.; Garrison, L. M.; Buchenauer, D. A.; Hatano, Y. Deuterium retention in neutron-irradiated single-crystal tungsten. *Fusion Eng. Des.* **2018**, *136*, 1161−1167.
(45) Koyanagi, T.; Kumar, N. A. P. K.; Hwang, T.; Garrison, L. M.; Hu, X.; Snead, L. L.; Katoh, Y. Microstructural evolution of pure tungsten neutron irradiated with a mixed energy spectrum. *J. Nucl. Mater.* **2017**, *490*, 66−74.
(46) Garrison, L. M.; Katoh, Y.; Kumar, N. A. P. K. Mechanical properties of single-crystal tungsten irradiated in a mixed spectrum fission reactor. *J. Nucl. Mater.* **2019**, *518*, 208−225.
(47) Katoh, Y.; Snead, L. L.; Garrison, L. M.; Hu, X.; Koyanagi, T.; Parish, C. M.; Edmondson, P. D.; Fukuda, M.; Hwang, T.; Tanaka, T.; Hasegawa, A. Response of unalloyed tungsten to mixed spectrum neutrons. *J. Nucl. Mater.* **2019**, *520*, 193−207.
(48) Hu, X.; Parish, C. M.; Wang, K.; Koyanagi, T.; Eftink, B. P.; Katoh, Y. Transmutation-induced precipitation in tungsten irradiated with a mixed energy neutron spectrum. *Acta Mater.* **2019**, *165*, 51−61.
(49) Hu, X.; Koyanagi, T.; Fukuda, M.; Katoh, Y.; Snead, L. L.; Wirth, B. D. Defect evolution in single crystalline tungsten following low temperature and low dose neutron irradiation. *J. Nucl. Mater.* **2016**, *470*, 278−289.
(50) Hu, X.; Koyanagi, T.; Fukuda, M.; Kumar, N. A. P. K.; Snead, L. L.; Wirth, B. D.; Katoh, Y. Irradiation hardening of pure tungsten exposed to neutron irradiation. *J. Nucl. Mater.* **2016**, *480*, 235−243.
(51) Shimada, M.; Hara, M.; Otsuka, T.; Oya, Y.; Hatano, Y. Defect annealing and thermal desorption of deuterium in low dose HFIR neutron-irradiated tungsten. *J. Nucl. Mater.* **2015**, *463*, 1005−1008.
(52) Hasegawa, A.; Fukuda, M.; Yabuuchi, K.; Nogami, S. Neutron irradiation effects on the microstructural development of tungsten and tungsten alloys. *J. Nucl. Mater.* **2016**, *471*, 175−183.
(53) Li, Y.; Gao, Y.; Xiao, B.; Min, T.; Fan, Z.; Ma, S.; Xu, L. Theoretical study on the stability, elasticity, hardness and electronic structures of W-C binary compounds. *J. Alloys Compd.* **2010**, *502* (1), 28−37.
(54) Kong, X.-S.; You, Y.-W.; Xia, J. H.; Liu, C. S.; Fang, Q. F.; Luo, G.-N.; Huang, Q.-Y. First principles study of intrinsic defects in hexagonal tungsten carbide. *J. Nucl. Mater.* **2010**, *406* (3), 323−329.
(55) Medvedeva, N. I.; Ivanovskii, A. L. Effect of metal and carbon vacancies on the band structure of hexagonal tungsten carbide. *Phys. Solid State* **2001**, *43* (3), 469−472.
(56) Lasa, A.; Björkas, C.; Vörtler, K.; Nordlund, K. MD simulations of low energy deuterium irradiation on W, WC and W2C surfaces. *J. Nucl. Mater.* **2012**, *429* (1−3), 284−292.
(57) Träskelin, P.; Björkas, C.; Juslin, N.; Vörtler, K.; Nordlund, K. Radiation damage in WC studied with MD simulations. *Nucl. Instrum. Methods Phys. Res., Sect. B* **2007**, *257* (1−2), 614−617.
(58) Juslin, N.; Erhart, P.; Träskelin, P.; Nord, J.; Henriksson, K.; Salonen, E.; Nordlund, K.; Albe, K. Analytical interatomic potential for modeling nonequilibrium processes in the W-C-H system. *J. Appl. Phys.* **2005**, *98* (12), 123520.
(59) Vörtler, K.; Nordlund, K. Molecular dynamics simulations of deuterium trapping and re-emission in tungsten carbide. *J. Phys. Chem. C* **2010**, *114* (12), 5382−5390.
(60) Kong, X. S.; You, Y. W.; Liu, C. S.; Fang, Q. F.; Chen, J. L.; Luo, G. N. First principles study of hydrogen behaviors in hexagonal tungsten carbide. *J. Nucl. Mater.* **2011**, *418* (1−3), 233−238.
(61) Kresse, G.; Furthmüller, J. Efficiency of ab-initio total energy calculations for metals and semiconductors using a plane-wave basis set. *Comput. Mater. Sci.* **1996**, *6* (1), 15−50.
(62) Kresse, G.; Furthmüller, J. Efficient iterative schemes for ab initio total-energy calculations using a plane-wave basis set. *Phys. Rev. B: Condens. Matter Mater. Phys.* **1996**, *54* (16), 11169−11186.
(63) Perdew, J. P.; Burke, K.; Ernzerhof, M. Generalized Gradient Approximation Made Simple. *Phys. Rev. Lett.* **1996**, *77* (18), 3865−3868.

DOI: 10.1021/acsaem.9b01990
ACS Appl. Energy Mater. 2020, 3, 868−878

(64) Grimme, S.; Ehrlich, S.; Goerigk, L. Effect of the damping function in dispersion corrected density functional theory. *J. Comput. Chem.* **2011**, *32* (7), 1456−1465.
(65) Yu, X. X.; Thompson, G. B.; Weinberger, C. R. Influence of carbon vacancy formation on the elastic constants and hardening mechanisms in transition metal carbides. *J. Eur. Ceram. Soc.* **2015**, *35* (1), 95−103.
(66) Barone, V.; Casarin, M.; Forrer, D.; Pavone, M.; Sambi, M.; Vittadini, A. Role and effective treatment of dispersive forces in materials: Polyethylene and graphite crystals as test cases. *J. Comput. Chem.* **2009**, *30* (6), 934−939.
(67) Kresse, G.; Joubert, D. From ultrasoft pseudopotentials to the projector augmented-wave method. *Phys. Rev. B: Condens. Matter Mater. Phys.* **1999**, *59* (3), 1758−1775.
(68) Methfessel, M.; Paxton, A. High-precision sampling for Brillouin-zone integration in metals. *Phys. Rev. B: Condens. Matter Mater. Phys.* **1989**, *40* (6), 3616−3621.
(69) Varvenne, C.; Bruneval, F.; Marinica, M.-C.; Clouet, E. Point defect modeling in materials: Coupling ab initio and elasticity approaches. *Phys. Rev. B: Condens. Matter Mater. Phys.* **2013**, *88* (13), 134102.
(70) Monkhorst, H. J.; Pack, J. D. Special points for Brillouin-zone integrations. *Phys. Rev. B* **1976**, *13* (12), 5188−5192.
(71) Frisk, K.; Dumitrescu, L.; Ekroth, M.; Sunduman, B.; Jansson, B.; Kruse, O. Development of a database for cemented carbides: Thermodynamic modeling and experiments. *J. Phase Equilib.* **2001**, *22*, 645−655.
(72) Velikanova, T. Y.; Eremenko, V. N. Phase equilibria in the ternary systems formed by molybdenum and tungsten with the groups IV and V transition metals and carbon. *Sov. Powder Metall. Met. Ceram.* **1974**, *13*, 293−297.
(73) Rudy, E. *Ternary Phase Equilibria in Transition Metal-Boron-Carbon-Silicon Systems. PART V. Compendium of Phase Diagram Data*. Aerojet-General Corp, 1969.
(74) Holleck, H. Die Konstitution ternaerer Systeme der Uebergangsmetalle der 4, 5, und 6. Gruppe mit Rhenium oder Platinmetallen und Kohlenstoff.-Teil I. *Metall* **1983**, 475.
(75) Fries, R. J.; Cummings, J. E.; Hoffman, C. G.; Daily, S. A. Carbide layer-growth rates on tungsten-molybdenum and tungsten-rhenium alloys. *J. Nucl. Mater.* **1971**, *39*, 35−48.
(76) Kuz'ma, Y. B.; Lakh, V. I.; Markiv, V. Y.; Stadnyk, B. I.; Gladyshevskii, E. I. X-ray diffraction study of the system tungsten-rhenium-carbon. *Sov. Powder Metall. Met. Ceram.* **1964**, *2*, 286−292.
(77) Holleck, H. Die Konstitution ternaerer Systeme der Uebergangsmetalle der 4, 5, und 6. Gruppe mit Rhenium oder Platinmetallen und Kohlenstoff. - Teil II. *Metall* **1983**, 475.
(78) Kröger, F. A.; Vink, H. J. Relations between the concentrations of imperfections in crystalline solids. *J. Phys. Chem. Solids* **1958**, *5* (3), 208−223.
(79) Whiting, T. M.; Burr, P. A.; King, D. J. M.; Wenman, M. R. Understanding the importance of the energetics of Mn, Ni, Cu, Si and vacancy triplet clusters in bcc Fe. *J. Appl. Phys.* **2019**, *126*, 115901.
(80) Popova, S. V. The crystal structures of new superconducting materials obtained by high pressure treatment. *Acta Crystallogr. Sect. A Cryst. Physics, Diffraction, Theor. Gen. Crystallogr.* **1975**, *31*, 99.
(81) Kempter, C. P.; Nadler, M. R. Preparation and crystal structures of RuC and OsC. *J. Chem. Phys.* **1960**, *33*, 1580.
(82) Obbard, E. G.; Luyckx, S.; Hamar-Thibault, S.; Allibert, C. H. Determination of the composition range suitable to the formation of WC-(V,W)Cx-Co materials. *Int. J. Refract. Hard Met.* **2001**, *19*, 349−357.

DOI: 10.1021/acsaem.9b01990
ACS Appl. Energy Mater. 2020, 3, 868−878